Journal of Computations & Modelling, vol.7, no.4, 2017, 1-20
ISSN: 1792-7625 (print), 1792-8850 (online)
Scienpress Ltd, 2017

Conservative finite volume element scheme for the regularized long wave equation

Quanxiang Wang[1]

Abstract

In this paper, a conservative finite volume element scheme for solving the regularized long wave equation is presented. Theoretical analysis shows that the proposed scheme can conserve the mass and energy. The efficiency of the scheme is illustrated by simulating propagation of single solitary wave, interaction of two solitary waves and undular bores. Numerical results indicate that this scheme is second-order accuracy in space and time, and has good conservation properties.

Mathematics Subject Classification: 65N12; 76D07
Keywords: conservative; RLW equation; finite volume element

1 Introduction

The regularized long wave (RLW) equation has been proposed by Peregrine [1] to describe the nonlinear dispersive waves. It has been shown that the

[1] College of Engineering, Nanjing Agricultural University, Nanjing 210031, China.
E-mail: wangqx@njau.edu.cn

Article Info: *Received* : August 11, 2017. *Revised* : September 9, 2017.
Published online : October 31, 2017.

equation governs a great number of important physical phenomena, such as the nonlinear transverse waves in shallow water and ionacoustic waves in plasma [2]. Because of the balance between nonlinear and dispersive effects, these waves preserve a stable waveform.

The RLW equation derived for long waves propagating in the positive x direction, is given by

$$u_t + u_x + \varepsilon u u_x - \mu u_{xxt} = 0, x \in [a, b], \tag{1}$$

where ε and μ are positive parameters, the subscripts x and t denote differentiation and the boundary condition is $u \to 0$ as $x \to \pm\infty$. In this paper, we will adopt periodic boundary conditions for the equation.

Benjamin et al. [3], have studied the mathematical theory of this equation as a regularized version of the Korteweg-de Viries equation. Olver [4] has shown that the RLW equation possesses only three conservation quantities corresponding to mass, momentum and energy

$$I_1 = \int_a^b u dx, \tag{2}$$

$$I_2 = \int_a^b \left(u^2 + (\mu u_x)^2\right) dx, \tag{3}$$

$$I_3 = \int_a^b \left(\varepsilon u^3 + 3u^2\right) dx, \tag{4}$$

respectively.

The RLW equation has been the subject of extensive investigations and a large number of numerical schemes have been designed to study it. For example, Peregrine [1] has proposed a simple finite difference scheme which is first-order accurate in time. Jain et al. [5] combined a splitting method and cubic spline technique to solve the RLW equation. Gardner et al. [6] solved the RLW equation using a least-squares technique and linear space-time finite elements. Zaki [7] has used splitting method and the cubic B-spline finite elements to solve the RLW equation. Dağ [8] has combined the quadratic B-spline functions with the least-squares method to solve the RLW equation. Cubic and quintic B-spline functions have also been used to develop a collocation method to solve the RLW equation [9,10]. Dogan [11] has solved the RLW equation using linear finite elements within Galerkin's method. Recently, Mei and Chen [12] proposed a new Galerkin method for the equation.

The finite volume element method has been one of the most commonly used numerical methods for solving partial differential equations. One main attractive property of the method is that, the mass conservation law is maintained, which is fairly desirable for fluid and underground fluid computations. So it has been extensively used in computational fluid dynamics [13-18].

In this study, we propose a conservative finite volume element scheme for the RLW equation. It has been shown that the scheme can conserve mass and energy of the RLW equation. The numerical scheme is derived based on the discrete variational derivative method (DVDM). Furihata has used the DVDM to design a stable finite difference scheme for the Cahn-Hilliard equation [19]. Further, Matsuo et al., [20,21] have extended the method to solve nonlinear Klein-Gordon equation and Degasperis-Procesi equation.

This paper is organized as follows. In Section 2, preliminaries and notations are introduced. In Section 3, the proposed conservative finite volume element scheme is presented. Some numerical experiments are provided to illustrate the effectiveness and accuracy of the proposed scheme in Section 4. We conclude the paper in Section 5.

2 Preliminaries and notations

Definition 2.1. *This is a text of a definition.*

$$ax + by + c = 0.$$

In this section, we introduce notations and useful propositions employed in this paper.

2.1 Trial and test function spaces

The region of interest $[a, b]$ can be decomposed into a grid T_h with nodes

$$a = x_0 < x_1 < x_2 < \cdots < x_{N-1} < x_N = b. \tag{5}$$

where $x_i - x_{i-1} = h$ and $h = \frac{b-a}{N}$. Denote $T_h = \{I_i : I_i = [x_{i-1}, x_i], i = 1, 2, \cdots N\}$. Accordingly we place a dual grid T_h^* with nodes

$$a = x_0 < x_{1/2} < x_{3/2} < \cdots < x_{N-3/2} < x_{N-1/2} < x_N = b, \tag{6}$$

where $x_{i-1/2} = x_i - h/2, (i = 1, 2, \cdots, N)$. Denote $I_0^* = [x_0, x_{1/2}]$, $I_i^* = [x_{i-1/2}, x_{i+1/2}]$ and $I_N^* = [x_{N-1/2}, x_N]$.

Select the trial function space U_h as the linear element space with respect to T_h. The basis function of the node x_i is

$$\phi_i(x) = \begin{cases} 1 - \mid x - x_i \mid /h, & x_{i-1} \leq x \leq x_{i+1}, \\ 0, & \text{elsewhere.} \end{cases} \tag{7}$$

Then numerical solution U for Eq. (1) can be uniquely written as $U = \sum_{i=1}^{N} U_i \phi_i(x)$, where $U_i = U(x_i, t)$. So in the element I_i, we have

$$U = U_{i-1}(1 - \chi) + U_i \chi, \tag{8}$$

$$U' = (U_i - U_{i-1})/h, \tag{9}$$

where $\chi = (x - x_{i-1})/h$.

The test function space V_h corresponding to T_h^* is taken as the piecewise constant function space. The test function of the nodes x_j is

$$\psi_j(x) = \begin{cases} 1, & x_{j-1/2} \leq x \leq x_{j+1/2}, \\ 0, & \text{elsewhere,} \end{cases} \tag{10}$$

The numerical solution is denoted by $U_k^n \simeq u(kh, n\Delta t)$, where Δt is the time step. For the regularized long wave equation, we adopt the following periodic boundary conditions

$$\frac{\partial^{m+l} u}{\partial x^m \partial t^l}\Big|_{x=a} = \frac{\partial^{m+l} u}{\partial x^m \partial t^l}\Big|_{x=b}, (m, l = 0, 1). \tag{11}$$

So the discrete periodic boundary conditions are

$$U_k^n = U_{k \bmod N}^n \text{ for } \forall k \in \mathbf{Z}. \tag{12}$$

2.2 Conserved quantities

In order to see the conservation property, it is convenient to work with the following representation

$$u_t - \mu u_{xxt} = -\frac{\partial}{\partial x}\left(\frac{\delta G}{\delta u}\right), \tag{13}$$

where $\frac{\delta G}{\delta u}$ is the Euler-Lagrange variational derivative defined by

$$\frac{\delta G}{\delta u} = \frac{\partial G}{\partial u} - \frac{\partial}{\partial x}\left(\frac{\delta G}{\delta u_x}\right)$$

and $G = \frac{u^2}{2} + \frac{\varepsilon}{6}u^3$.

Proposition 1. *Let u be the solution of Eq. (13). Then the total mass $I_1 = \int_a^b u dx$ is independent of t. Namely,*

$$\frac{dI_1}{dt} = 0. \tag{14}$$

Proposition 2. *Let u be the solution of Eq. (13). Then the total energy $I_3 = \int_a^b \left(\varepsilon u^3 + 3u^2\right) dx$ is independent of t. Namely,*

$$\frac{dI_3}{dt} = 0. \tag{15}$$

Proof According to the chain rule, we have

$$\frac{1}{6}\frac{dI_3}{dt} = \int_a^b \frac{\delta G}{\delta u} u_t dx.$$

By the Eq. (13), we can get

$$\begin{aligned}
\frac{1}{6}\frac{dI_3}{dt} &= \int_a^b \left[\left(\frac{\delta G}{\delta u} - \mu u_{xt}\right) u_t + \mu u_{xt} u_t\right] dx \\
&= \int_a^b \left[-\left(\mu u_{xt} - \frac{\delta G}{\delta u}\right)\frac{\partial}{\partial x}\left(\mu u_{xt} - \frac{\delta G}{\delta u}\right) + \frac{\mu}{2}\frac{\partial}{\partial x}\left(u_t\right)^2\right] dx \\
&= \frac{1}{2}\int_a^b \frac{\partial}{\partial x}\left[-\left(\mu u_{xt} - \frac{\delta G}{\delta u}\right)^2 + \mu\left(u_t\right)^2\right] dx \\
&= \frac{1}{2}\left[-\left(\mu u_{xt} - \frac{\delta G}{\delta u}\right)^2 + \mu\left(u_t\right)^2\right]_a^b.
\end{aligned}$$

At last, we can complete the proof using the Eq. (11).

3 Design of schemes

3.1 Discrete variational derivative method

In the following, we recall the discrete variational derivative method briefly.

Firstly, we define the energy as follows:

$$J(u) = \int_a^b G(u)dx, \tag{16}$$

where we call G the energy function throughout this paper. As the discretization of energy function, we employ the following finite volume element approximation

$$G_d(U) \simeq G, \tag{17}$$

Then we define the total discrete energy as follows:

$$J(u) = \int_a^b G_d(U)dx, \tag{18}$$

To obtain the approximation $\frac{\delta G_d}{\delta(U,V)}$ of Euler-Lagrange derivative $\frac{\delta G}{\delta u}$, we need to compute the following difference:

$$J(U) - J(V) = \int_a^b \frac{\delta G_d}{\delta(U,V)}(U-V)dx. \tag{19}$$

3.2 Conservative finite volume element scheme

Using any $\psi \in V_h$ to multiply both sides of Eq. (13) and integrating on the interval $[a,b]$, we can obtain the following semi-discrete scheme

$$\left(\left(1-\mu\partial_x^2\right)u_t, \psi\right) = \left(-\frac{\partial}{\partial x}\left(\frac{\delta G}{\delta u}\right), \psi\right), \tag{20}$$

where $(\cdot,\cdot)$ denotes the inner product of $L^2([a,b])$.

Now we discretize the above semi-discrete scheme in time. To simplify the notation, we will use the difference operator $\delta_n^{\langle 1\rangle}u^n = \frac{u^{n+1}-u^{n-1}}{2\Delta t}$. Additionally, we define the discrete version of Euler-Lagrange derivative $\frac{\delta G}{\delta u} = u + \frac{\varepsilon}{2}u^2$ by

$$\frac{\delta G_d}{\delta(u^{n+1},u^n,u^{n-1})} = u^n + \frac{\varepsilon u^n(u^{n+1}+u^n+u^{n-1})}{6}. \tag{21}$$

At last, we can get the following conservative finite volume element scheme

$$\left(\left(1-\mu\partial_x^2\right)\delta_n^{\langle 1\rangle}u^n, \psi\right) = \left(-\frac{\partial}{\partial x}\left(\frac{\delta G_d}{\delta(u^{n+1},u^n,u^{n-1})}\right), \psi\right). \tag{22}$$

The Eq. (22) has the following discrete mass and energy conservation law.

Theorem 1. *(Discrete mass conservation law). Under the discrete periodic boundary condition, then numerical solution by Eq. (22) conserves mass*

$$\int_a^b u^n dx = const. \tag{23}$$

Theorem 2. *(Discrete energy conservation law). Under the discrete periodic boundary condition, then numerical solution by Eq. (22) conserves energy*

$$6\int_a^b G_d^n dx = const. \tag{24}$$

Proof

$$\begin{aligned}
&\frac{1}{\Delta t}\int_a^b \left(G_d^{n+1} - G_d^n\right) dx \\
&= \left(\frac{\delta \tilde{G}_d}{\delta(u^{n+1}, u^n, u^{n-1})}, \delta_n^{\langle 1\rangle} u^n\right) \\
&= \left(\frac{\delta \tilde{G}_d}{\delta(u^{n+1}, u^n, u^{n-1})} - \mu\partial_x\delta_n^{\langle 1\rangle} u^n + \mu\partial_x\delta_n^{\langle 1\rangle} u^n, \delta_n^{\langle 1\rangle} u^n\right) \\
&= \left(\frac{\delta \tilde{G}_d}{\delta(u^{n+1}, u^n, u^{n-1})} - \mu\partial_x\delta_n^{\langle 1\rangle} u^n, \delta_n^{\langle 1\rangle} u^n\right) + \left(\mu\partial_x\delta_n^{\langle 1\rangle} u^n, \delta_n^{\langle 1\rangle} u^n\right) \\
&= \left(\frac{\delta \tilde{G}_d}{\delta(u^{n+1}, u^n, u^{n-1})} - \mu\partial_x\delta_n^{\langle 1\rangle} u^n, \frac{\partial}{\partial x}\left(\frac{\delta G_d}{\delta(u^{n+1}, u^n, u^{n-1})} - \mu\partial_x\delta_n^{\langle 1\rangle} u^n\right)\right) \\
&+ \left(\mu\partial_x\delta_n^{\langle 1\rangle} u^n, \delta_n^{\langle 1\rangle} u^n\right).
\end{aligned}$$

At last, we can complete the proof using the periodic boundary conditions.

4 Numerical experiments

In this section, we solve three test problems to demonstrate the efficiency of the proposed conservative finite volume element scheme. In order to check the accuracy of the scheme, we compute L_2 and L_∞ error norms defined as follows

$$L_2 = \sqrt{\sum_{i=1}^{N} |U_i - u_i|^2 h}, \tag{25}$$

Table 1: Error norms for single solitary wave, $c = 0.1$.

h	Δt	L_∞	r	L_2	r
1/2	2/5	1.0647e-03	-	2.8143e-03	-
1/4	1/5	2.6628e-04	1.9994	7.0358e-04	2.0000
1/8	1/10	6.6611e-05	1.9991	1.7671e-04	1.9933
1/16	1/20	1.6665e-05	1.9989	4.7213e-05	1.9041

$$L_\infty = \max_i |U_i - u_i|. \tag{26}$$

Additionally, we define the convergence rate r

$$r = \log_2(\frac{||U_{2h} - u||}{||U_h - u||}),$$

where U_h is the numerical solution with space step h, u the analytical solution, N the number of node. The rate approaches the number 2 would indicate second-order accuracy in space and time. We will monitor the conservation quantities of the RLW equation to examine the conserved properties of the numerical scheme.

4.1 Single solitary wave

Eq. (1) has the following analytical solution which describes solitary wave

$$u(x,t) = 3c \operatorname{sech}^2\left(k[x - x_0 - vt]\right), k = \frac{1}{2}\sqrt{\frac{\varepsilon c}{\mu(1+\varepsilon c)}}, \tag{27}$$

where $3c$ is amplitude of the solitary wave which is initially centered on $x = x_0$ traveling with velocity $v = 1 + \varepsilon c$. Setting $t = 0$, the initial condition is obtained

$$u(x,0) = 3c \operatorname{sech}^2\left(k[x - x_0]\right). \tag{28}$$

To compare our results with those given in other references, we will take $\varepsilon = \mu = 1.0$, $x_0 = 0$, $c = 0.1$, and solve the problem over the domain $[-40, 60]$ in the following.

In order to demonstrate the accuracy of our method, we have integrated the problem at various resolutions up to time $t = 20$. The L_2 and L_∞ error

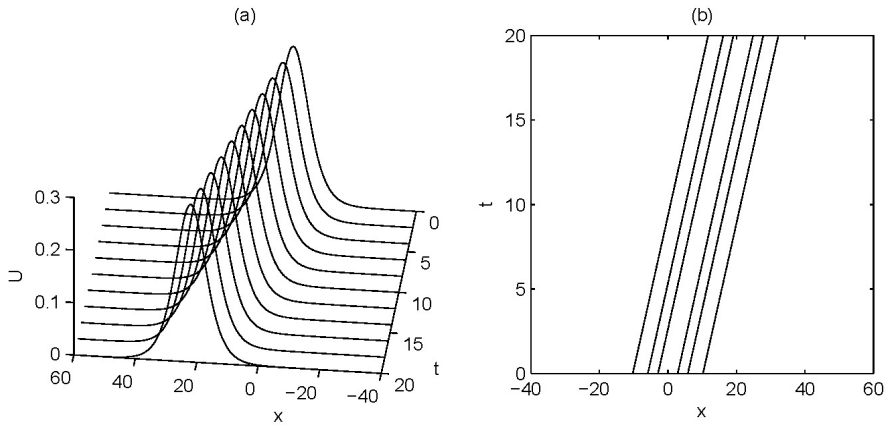

Figure 1: The propagation for single solitary wave, $c = 0.1$.

norms for u have been computed by conservative finite volume element scheme. They are displayed in Table 1. Examination of the table shows that the error measures of our method diminish approximately quadratically as the space and time step are simultaneously halved. In other words, the proposed finite volume element scheme is second-order accuracy in space and time.

We perform a simulation with space step $h = 1/8$ and time step $\Delta t = 1/10$ for single solitary wave on the time interval $[0, 20]$. Figure 1 presents that the solitary wave propagates towards the right without change in form. It is easy to find that the solitary wave continues to evolve with the initial velocity. We also perform a simulation with the resolution to check the conservation of our scheme. Figure 2 presents the error in the discrete mass and energy for the proposed scheme. From the figure, we can find that our scheme can conserve mass and energy within 10^{-13}, which is strict conservation in numerical sense and conforms the theoretical result.

To make comparison with the earlier works, we compute invariants and error norms for single solitary wave with $h = 1/8$ and $\Delta t = 1/10$ up to $t = 20$. The previous results are also listed in Table 2. It is deduced from the L_∞ error norm and conserved quantities that our scheme performs the motion of single solitary wave satisfactorily. For example, the proposed scheme provides smaller error than those presented in [9,10,12] . Additionally, the discrete mass and energy are constant during the simulation. The discrete momentum is conserved within 10^{-6} which is satisfactory.

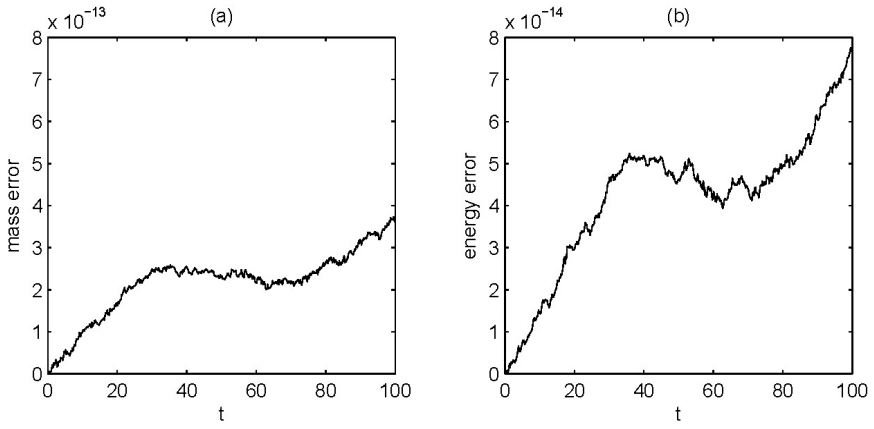

Figure 2: (a) Error in the discrete mass; (b) Error in the discrete energy. Single solitary wave.

Table 2: Invariants and error norms for single solitary wave, $h = 1/8$ and $\Delta t = 1/10$.

Method	Time	L_∞	I_1	I_2	I_3
Analytical		0	3.979949748	0.810462494	2.579007437
Our method	0	0	3.979927104	0.810360229	2.578672806
	20	6.6611e-05	3.979927104	0.810360998	2.578672806
[9]	0	0	3.979927	0.81046251	2.57900750
	20	1.1600e-04	3.979883	0.81027618	2.57839258
[10]	0	0	3.9799271	0.8104625	2.5790075
	20	7.3370e-05	3.9798832	0.8104612	2.5790031
[12]	0	0	3.97993	0.81035	2.57901
	20	9.1465e-05	3.97972	0.81026	2.57873

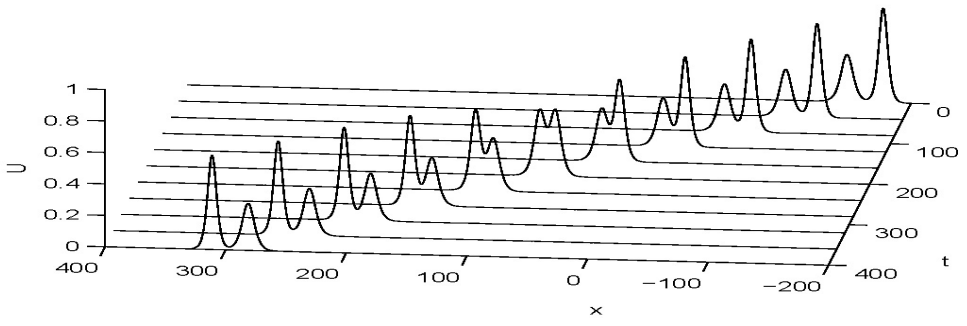

Figure 3: The propagation for two solitary waves. $c_1 = 0.2$, $c_2 = 0.1$, $h = 1/8$, $\Delta t = 1/10$.

4.2 Two solitary waves

In this section, the interaction of two solitary waves is studied by using the following initial conditions

$$u(x,0) = 3c_1 \operatorname{sech}^2\left(k_1[x - x_{01}]\right) + 3c_2 \operatorname{sech}^2\left(k_2[x - x_{02}]\right), \tag{29}$$

where $k_1 = \frac{1}{2}\sqrt{\frac{\varepsilon c_1}{\mu(1+\varepsilon c_1)}}$, $k_2 = \frac{1}{2}\sqrt{\frac{\varepsilon c_2}{\mu(1+\varepsilon c_2)}}$. The parameters ε and μ are taken as 0.1.

Firstly, we study the behavior of the interaction of two solitary waves having different amplitudes and travelling in the same direction. In order to compare our method with eariler results, we will solve the RLW equation over the region [-200,400] with $x_{01} = -177$, $x_{02} = -147$, $c_1 = 0.2$ and $c_2 = 0.1$. The experiment is run from $t = 0$ to $t = 400$ to allow the interaction to take place. Figure 3 shows the interaction of two positive solitary waves. Figure 4 presents the error in the discrete mass and energy for the proposed scheme. It is observed that our scheme can conserve mass and energy within 10^{-12}, which is also strict conservation in numerical sense and conforms the theoretical analysis. Numerical results in Table 3 shows the comparison of the conserved quantities I_1, I_2 and I_3 obtained by our scheme with previous results [11,12]. From the table, we can observe that the mass and energy are not changed during the interaction of the two solitary waves and the conservation is best in our method.

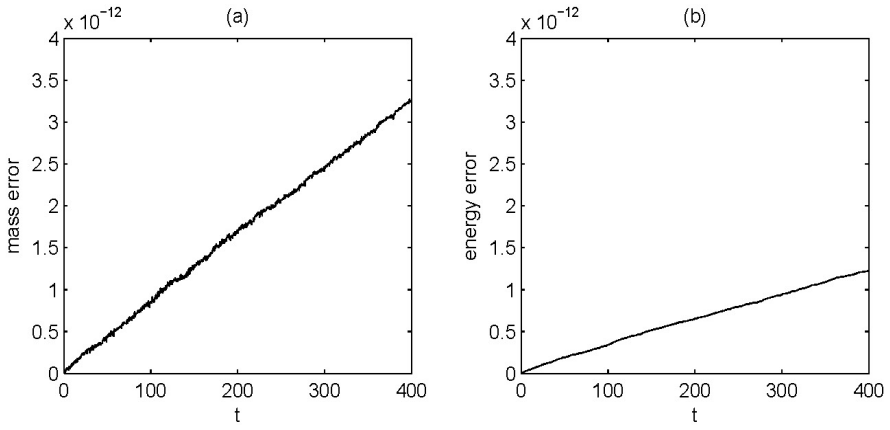

Figure 4: (a) Error in the discrete mass; (b) Error in the discrete energy. Two solitary waves.

Table 3: Invariants for two solitary waves. $c_1 = 0.2$ and $c_2 = 0.1$.

Method	Time	I_1	I_2	I_3
Analytical		9.858725131	3.240356319	10.76226277
Our method	0	9.858258030	3.243206628	10.77312299
	200	9.858258030	3.243814635	10.77312299
	400	9.858258030	3.243289136	10.77312299
[11]	0	9.8586	3.2449	10.7788
	200	9.8786	3.2523	10.8036
	400	9.8930	3.2585	10.8251
[12]	0	9.8583	3.2328	10.7623
	200	9.8574	3.2384	10.7654
	400	9.8563	3.2351	10.7703

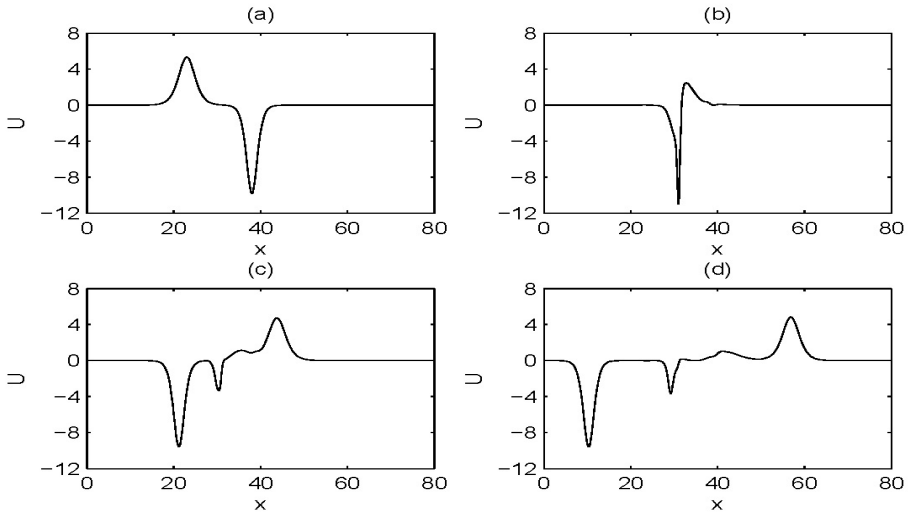

Figure 5: The propagation for two solitary waves at (a)$t = 0$, (b)$t = 5$, (c)$t = 10$ and (d)$t = 15$.

Now we simulate the interaction of a positive and negative solitary wave. In this case, the RLW equation is solved over the domain $[0, 80]$ and the parameters are chosen as $k_1 = 0.4$, $k_2 = 0.6$, $x_{01} = 23$ and $x_{02} = 38$. We perform a simulation with space step $h = 1/10$ and time step $\Delta t = 1/10$. Figure 5 shows the interaction of the two solitary waves and it is observed that there are at least two additional solitary waves produced, which is consistent with the results in [22,23].

At last, we study the interaction of two negative solitary waves over the region $[0, 120]$ with $k_1 = 0.6$, $k_2 = 0.8$, $x_{01} = 82$, $x_{02} = 67$, $h = \Delta t = 1/10$. The process of interaction is presented in Figure 6 and additional solitary waves are also produced. Hence the interaction is inelastic and this is in good agreement with those reported in [22].

4.3 Wave undulation

In this subsection, we consider the development of an undular bore with the initial condition

$$u(x, 0) = \frac{1}{2} u_0 \left[1 - \tanh \left(\frac{x - x_c}{d} \right) \right], \tag{30}$$

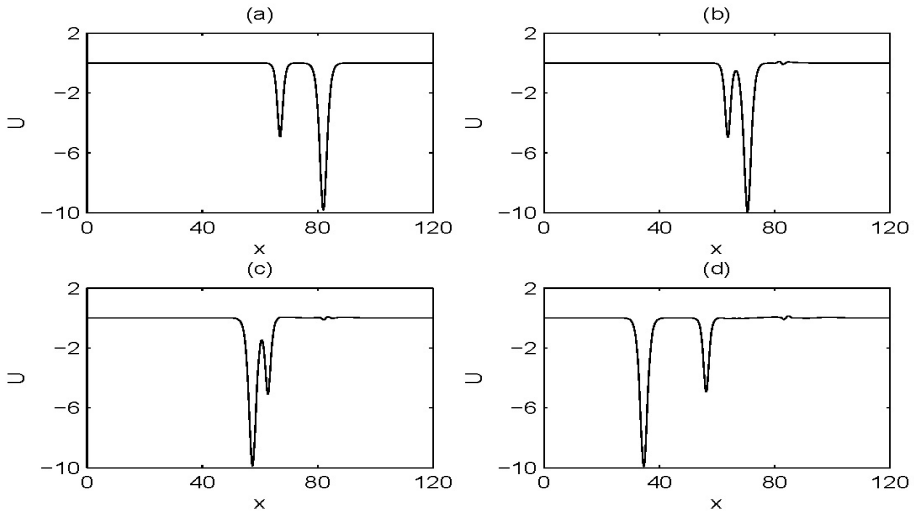

Figure 6: The propagation for two solitary waves at (a)$t = 0$, (b)$t = 5$, (c)$t = 10$ and (d)$t = 20$.

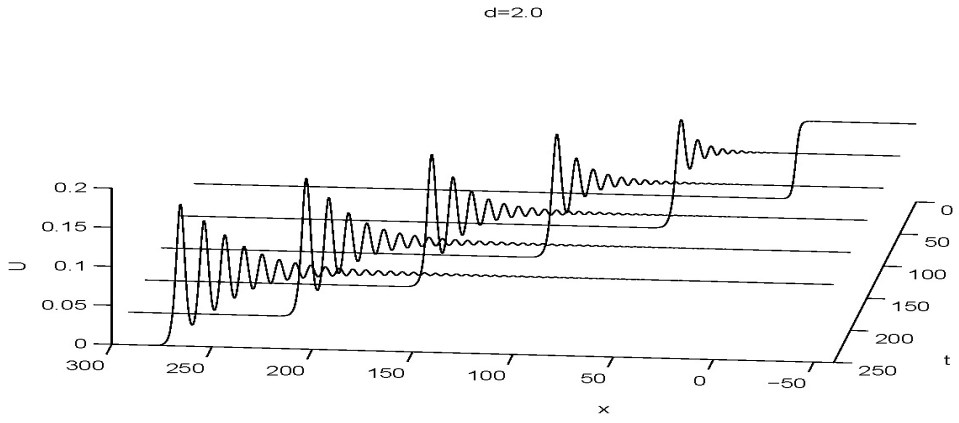

Figure 7: The development of undular bore for steep slope $d = 2.0$.

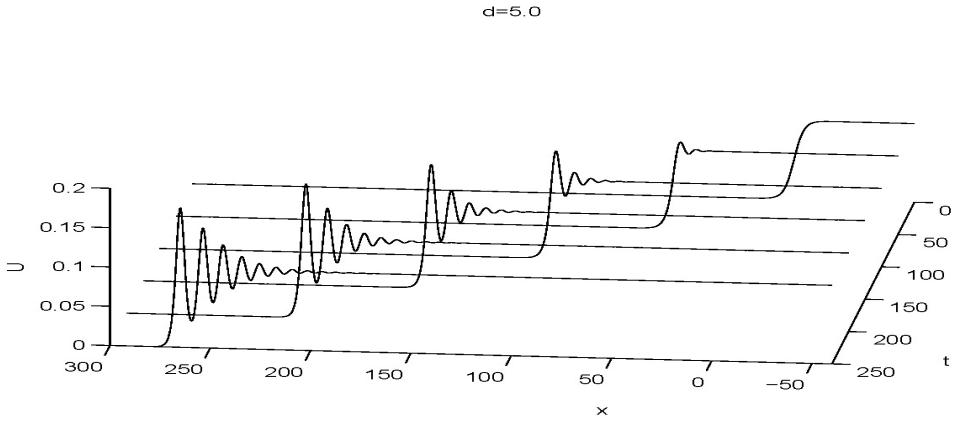

Figure 8: The development of undular bore for gentle slope $d = 5.0$.

where $u(x, 0)$ denotes the elevation of the water above the equilibrium surface at $t = 0$, u_0 denotes the magnitude of the change in water level which is centered on $x = x_c$. For the undular bore, d represents the slope between the still water and deeper water.

For comparison with earlier studies, we take $\varepsilon = 1.5$, $\mu = 1/6$, $u_0 = 0.1$, $x_0 = 0$. The problem is solved over the range $[-60, 300]$ up to $t = 250$ with space step $h = 0.24$ and time step $\Delta t = 0.1$. In addition, the boundary conditions have been chosen as $u = u_0$ for $x = -60$ and $u = 0$ for $x = 300$.

Figure 7 and 8 present the development of the undular bore at various times from $t = 0$ to $t = 250$ for steep slope $d = 2.0$ and gentle slope $d = 5.0$, respectively. It is observed that there is no instability during the undulation process. Amplitudes and positions of first two peaks are given in Table 4. From the table, we can find that the undulations are almost travelled with the same velocity and amplitude will increase when steep slope is considered. So we can conclude that the slopes only have an effect on amplitudes. The results are consistent with previous works [9,12]. The growth change of the leading undulation for both steep and gentle slopes are shown in Figure 9. It can be seen that the formation of the first undulation is almost at $t = 3$ and the rate of growth is fast in the beginning and then decreases slowly. For gentle slope, the first undulation is formed at $t = 29$, as reported in [12].

In this case, the quantities I_1, I_2 and I_3 are no longer constant but increase

Table 4: Amplitudes and positions of undulations at $t = 250$.

	$d = 2.0$		$d = 5.0$	
	Position	Amplitude	Position	Amplitude
Our method				
Leading undulation	265.92	0.18175	265.20	0.17744
Second undulation	254.16	0.16156	253.92	0.15249
[9]				
Leading undulation	265.92	0.182	264.96	0.178
Second undulation	254.16	0.162	253.92	0.153
[12]				
Leading undulation	265.92	0.18225	265.20	0.17791
Second undulation	254.40	0.16230	253.92	0.15344

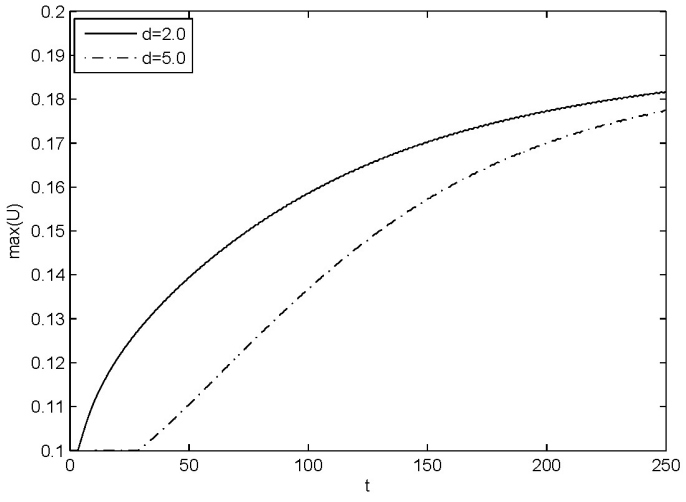

Figure 9: The development of leading undulation.

Table 5: The numerical results for M_1, M_2 and M_3.

	Time	M_1	M_2	M_3
Analytical		0.1050000	0.0106667	0.03307500
$d = 2.0$	50	0.1075000	0.0109898	0.03466875
	150	0.1075000	0.0109865	0.03466875
	250	0.1075000	0.0109851	0.03466875
$d = 5.0$	50	0.1075000	0.0109976	0.03466875
	150	0.1075000	0.0109926	0.03466875
	250	0.1075000	0.0109892	0.03466875

linearly throughout the simulation at the following rates

$$M_1 = \frac{dI_1}{dt} = \frac{d}{dt}\int_a^b u dx = u_0 + \frac{1}{2}u_0^2 = 0.105,$$

$$M_2 = \frac{dI_2}{dt} = \frac{d}{dt}\int_a^b \left(u^2 + (\mu u_x)^2\right) dx = u_0^2 + \frac{2}{3}u_0^2 = 0.0106667,$$

$$M_3 = \frac{dI_3}{dt} = \frac{d}{dt}\int_a^b \left(\varepsilon u^3 + 3u^2\right) dx = 3u_0^2 + 3u_0^3 + \frac{3}{4}u_0^4 = 0.033075. \quad (31)$$

The numerical results for M_1, M_2 and M_3 are given in Table 5 for $d = 2.0$ and $d = 5.0$. It is observed that the numerical growth rates of mass and energy are constant and there is no obvious change for the growth rates of momentum.

5 Conclusion

In this paper, the conservative finite volume element scheme is introduced for solving the initial boundary problems of the RLW equation. The conservation of the proposed numerical scheme is proved. The efficiency of the scheme is illustrated by simulating propagation of single solitary wave, interaction of two solitary waves and undular bores. Numerical results demonstrate that the proposed finite volume element scheme is second-order accuracy in space and time. Moreover, the new scheme can conserve mass and energy to machine accuracy. Since the present method is simple and efficient, it can also be used to solve other similar problems. This is our ongoing research.

ACKNOWLEDGEMENTS. This project is partially supported by the Fundamental Research Funds for the Central Universities No.KYZ201565, the National Natural Science Foundation of China grant Nos.11701283, 11426134, 11471166. The authors would like to thank the editors and the anonymous referees for their invaluable comments and suggestions which have helped to improve the paper greatly.

References

[1] D. Peregrine, Calculations of the development of an undular bore, *Journal of Fluid Mechanics*, **25**(2), (1966), 321-330.

[2] K.O. Abdulloev, I. Bogolubsky and V. Makhankov, One more example of inelastic soliton interaction, *Physics Letters*, **56**(6), (1976), 427-428.

[3] T.B. Benjamin, J.L. Bona and J.J. Mahony, Model equations for long waves in nonlinear dispersive systems, *Philosophical Transactions of the Royal Society of London. Series A, Mathematical and Physical Sciences*, **272**(1220), (1972), 47-78.

[4] P.J. Olver, Euler operators and conservation laws of the BBM equation, *Mathematical Proceedings of the Cambridge Philosophical Society*, **85**(1), (1979), 143-160.

[5] P. Jain, R. Shankar and T. Singh, Numerical solution of regularized long wave equation, *Communications in Numerical Methods in Engineering*, **9**(7), (1993), 579-586.

[6] L. Gardner, G. Gardner and A. Dogan, A least-squares finite element scheme for the RLW equation, *Communications in Numerical Methods in Engineering*, **12**(11), (1996), 795-804.

[7] S. Zaki, Solitary waves of the splitted RLW equation,*Computer Physics Communications*, **138**(1), (2001), 80-91.

[8] I. Dag, Least-squares quadratic B-spline finite element method for the regularised long wave equation, *Computer Methods in Applied Mechanics and Engineering*, **182**(1), (2000), 205-215.

[9] I. Dag, B. Saka and D. Irk, Application of cubic B-splines for numerical solution of the RLW equation, *Applied Mathematics and Computation*, **159**(2), (2004), 373-389.

[10] I. Dag, B. Saka and D. Irk, Galerkin method for the numerical solution of the RLW equation using quintic B-splines, *Journal of Computational and Applied Mathematics*, **190**(1), (2006), 532-547.

[11] A. Dogan, Numerical solution of RLW equation using linear finite elements within Glerkin's method, *Applied Mathematical Modelling*, **26**(7), (2002), 771-783.

[12] L. Mei and Y. Chen, Numerical solutions of RLW equation using Glerkin method with extrapolation techniques, *Computer Physics Communications*, **183**(8), (2012), 1609-1616.

[13] J. Xu and Q. Zou, Analysis of linear and quadratic simplical finite volume methods for elliptic equations, *Numerische Mathematik*, **111**(3), (2009), 469-492.

[14] Z. Zhang, Error estimates of finite volume element method for the pollution in groundwater flow, *Numerical Methods for Partial Differential Equations*, **25**(2), (2009), 259-274.

[15] Q. Wang, Z. Zhang and Z. Li, A Fourier finite volume element method for solving two-dimensional quasi-geostrophic equations on a sphere, *Applied Numerical Mathematics*, **71**, (2013), 1-13.

[16] Q. Wang, Z. Zhang and Q. Zhu, Numerical simulation of the stochastic damped improved Boussinesq equation, *Journal of Mathematical Physics*, **54**(1), (2013), 1-18.

[17] Q. Wang and Z. Zhang, High-order upwind finite volume element schemes for modelling of neuronal firing, *International Journal of Computer Mathematics*, **91**(3), (2014), 625-640.

[18] Z. Luo, A stabilized Crank-Nicolson mxed finite volume element formulation for the non-stationary incompressible Boussinesq equations, *Journal of Scientific Computing*, **66**(2), (2016), 555-576.

[19] D. Furihata, A stable and conservative finite difference scheme for the Cahn-Hilliard equation, *Numerische Mathematik*, **87**(4), (2001), 675-699.

[20] T. Matsuo, New conservative schemes with discrete variational derivatives for nonlinear wave equations, *Journal of Computational and Applied Mathematics*, **203**(1), (2007), 32-56.

[21] Y. Miyatake and T. Matsuo, Conservative finite difference schemes for the Degasperis-Procesi equation, *Journal of Computational and Applied Mathematics*, **236**(15), (2012), 3728-3740.

[22] K. Raslan. A computational method for the regularized long wave (RLW) equation, *Applied Mathematics and Computation*, **167**(2), (2005), 1101-1118.

[23] A. Santarelli, Numerical analysis of the regularized long-wave equation: anelastic collision of solitary waves, *Il Nuovo Cimento B Series 11*, **46**(1), (1978), 179-188.